LIQUID STRUCTURES AND PHYSICAL PROPERTIES – GROUND BASED STUDIES FOR ISS EXPERIMENTS

K. F. Kelton, J. C. Bendert, and N. A. Mauro

Department of Physics, Washington University, St. Louis, MO 63130

Abstract

Studies of electrostatically-levitated supercooled liquids have demonstrated strong short- and medium-range ordering in transition metal and alloy liquids, which can influence phase transitions like crystal nucleation and the glass transition. The structure is also related to the liquid properties. Planned ISS experiments will allow a deeper investigation of these results as well as the first investigations of a new type of coupling in crystal nucleation in primary crystallizing liquids, resulting from a linking of the stochastic processes of diffusion with interfacial-attachment. A brief description of the techniques used for ground-based studies and some results relevant to planned ISS investigations are discussed.

I.   Introduction

Fahrenheit [1] first demonstrated that under the right conditions water can be cooled far below its melting temperature without freezing, indicating a barrier to crystallization. That metallic liquids resisted supercooling was believed to indicate a small nucleation barrier, arising from similarities in the atomic structures of the liquid and crystal, a view supported by their similar densities and coordination numbers. However, if heterogeneous sites for nucleation are removed it is possible to deeply supercool liquid metals [2, 3]. This can be explained if undercooled liquids develop icosahedral short-range icosahedral order (ISRO), which is incompatible with crystalline periodicity [4]. Experimental data from liquids and glasses support this view [5-9]. This and subsequent work show that nucleation in liquids is more complicated than generally thought. It is well known that it can be coupled to other first-order processes, such as phase separation prior to crystallization and the precipitation of nano-sized heterogeneous sites, but these studies demonstrate that local order in a liquid can also couple to the nucleation barrier. Dynamical coupling effects can occur. For example, when the nucleating phase has a different chemical composition than that of the original phase, models predict that the interfacial flux, of central concern in the *classical theory of nucleation*, can couple to the long-range diffusion field [10, 11]. Ordering can also couple to atomistic dynamics, significantly influencing the nucleation kinetics and possibly giving rise to dynamical phase transitions, such as the fragile/strong transition.   A more thorough investigation of these processes requires a microgravity environment to minimize stirring effects and allow key thermophysical properties to be measured. As a member of the THERMOLAB and ICOPROSOL teams, we will carry out these studies on the International Space Station. To support those activities, we are making extensive ground-based studies of liquid structures and some thermophysical properties.   In this

manuscript, a brief overview of our ground-based techniques and activities and a brief review of some of the results obtained, are provided.

II.   X-Ray Diffraction of Supercooled Liquids

Electrostatic levitation (ESL) is used for containerless investigations of the high temperature liquids of interest; most of our studies are now made using the recently constructed Washington University Beamline ESL, or WU-BESL (Fig. 1). In ESL, charged samples (2.0 – 4.0 mm diameter) are levitated in an electrostatic field (0 to 2 MV/m) under high vacuum ($\approx 10^{-7}$torr). Three pairs of orthogonal electrodesand a robust control algorithm maintain the sample position during processing to better than 50μm. The samples are initially charged by induction and the charge is maintained during processing with an external UV source. Samples are melted using a 50 W diode laser and the sample temperature is measured across a range of 160 to 2300°C using a combination of two infrared pyrometers with overlapping ranges. In addition to structural studies, WU-BESL is capable of making coordinated density, viscosity and surface tension measurements. More details on WU-BESL can be found elsewhere [12].
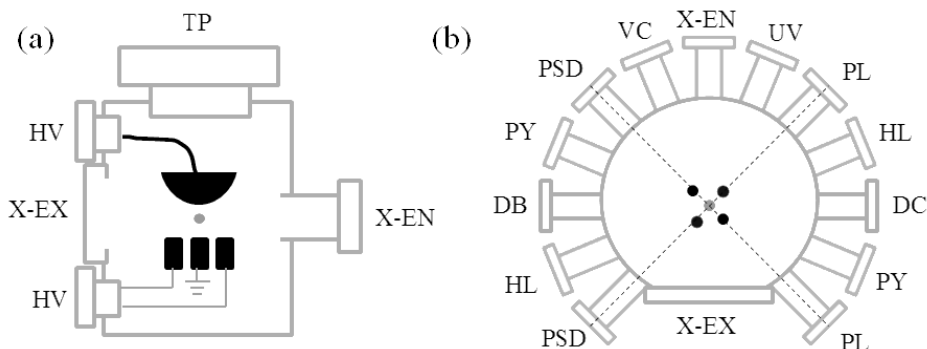
Figure 1 –Schematic drawing of the WU-BESL: (a) vertical and (b) horizontal cuts through the sample. The top and bottom electrode and two side electrodes are schematically indicated in (a) (solid black). Components: TP - turbo pump; HV - high voltage feed through; X-EN –X-ray entrance window; X-EX –X-ray exit window; PL - positioning laser; PSD - position sensitive detector, PY – pyrometer; DC – density camera; HL - heating laser; UV - ultra violet light source; VC - visualization camera; DB – backlight for density measurements.

X-ray scattering experiments are made in a transmission geometry (Fig. 2); a series of collimators and a beam-stop reduce the background to acceptable levels. For a typical study (E = 129keV, λ = 0.09611Å), useful data can be obtained to 15 Å^{-1} using a GE Revolution 41-RT amorphous Si flat panel X-ray detector at a sampling rate of up to 10 Hz.

The scattering data are used to obtain the total X-ray static structure factor, $S(q)$, from which structural information is inferred using either single cluster [7, 8] or Reverse Monte Carlo (RMC) [13, 14] approaches. When constrained with the measured liquid density and atomic sizes, an RMC fit yields a reasonable topological model for the liquid; it does not, however, yield realistic chemical correlations (such as the partial pair distribution functions). If the RMC can be

34

further constrained with information from molecular dynamics (MD) structural studies, elastic neutron diffraction, EXAFS, or anomalous scattering data, it becomes possible to obtain more accurate partial pair distribution functions. The order in the RMC structures is characterized using the Honeycutt-Andersen (HA) indices [15], bond orientation order parameters [16, 17] and Voronoi polyhedra (VI) construction [18]. The HA indices typically indicate a large amount of five-fold symmetry, which may not, however, signal complete icosahedral clusters. Consistent with this, the VI construction tends to show much smaller amounts of icosahedral order [19].
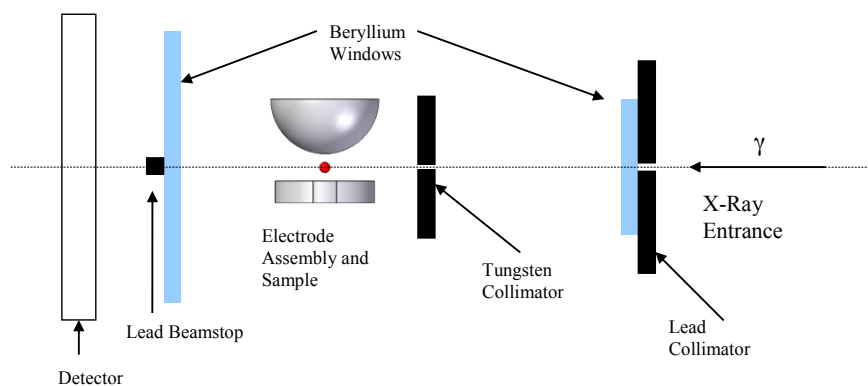
Figure 2 – Schematic of the X-ray optics in WU-BESL

Many studies indicate that icosahedral short-range order (ISRO) in metallic liquids increases with supercooling [7, 8, 20-22]. A developing shoulder on the high-q side of the second peak in $S(q)$ often correlates with ISRO. This is observed in the scattering data from liquid $Zr_{59}Ti_3Cu_{20}Ni_8Al_{10}$, abulk metallic glass former (Fig. 3.a). An increase in the number of 1551 HA indices from atomic structures obtained from a RMC fit to the scattering data (Fig. 3.b) supports this conclusion in this case. However, it is important to point out that a developing shoulder should only be used as a rough guide. Other local structures can produce a similar shoulder, and in some cases ISRO may be dominant with no evidence of the shoulder. The latter is the case for liquid Al, which shows no asymmetric second peak, yet an HA analysis of the RMC structures indicates a high degree of ISRO [23]. When present, ISRO can couple to the nucleation barrier [8] and may play a role in the glass transition in some cases [9].

Many reports exist of medium-range order (MRO) in glasses, i.e. ordering beyond nearest neighbors, [24-28]. In some case, evolution of MRO has been correlated with changes in plasticity [25] and viscosity [29]. Since reports of medium-range ordering in metal-metal liquids have been rare, it is of interest to determine under what conditions it can be observed. Binary liquids, such as Zr-Pd and Zr-Pt, provide good systems for such studies. The two alloys are very similar. Both have deep eutectics at similar Zr-rich compositions and both form glasses that devitrify first to the icosahedral quasicrystal phase [30]. Further, Pd and Pt have similar bonding properties with Zr and are of similar sizes. However, recent WU-BESL studies of the two eutectic liquids show qualitatively different X-ray static structure factors [31, 32]. As shown in Fig. 4, a pre-peak is clearly observed in the $S(q)$ data at all temperatures for $Zr_{80}Pt_{20}$ liquids (indicated by an arrow), while it is not observed in $Zr_{75.5}Pd_{24.5}$ liquids. Given the many similarities between these two systems, the presence of a pre-peak in one and not in the other is

at first difficult to understand. An analysis of constrained RMC fits to the data, made using partial pair-correlation functions obtained from MD simulations [31, 32] revealed a solute-solute (Pd-Pd or Pt-Pt) correlation in both cases, which manifests itself as a prepeak at ~1.7Å^{-1}. Because Pd has a much smaller atomic form factor than Pt, however, the correlation is not evident in the experimental X-ray data for Zr-Pd, suggesting that MRO may be much more common in metal-metal liquids than previously thought.
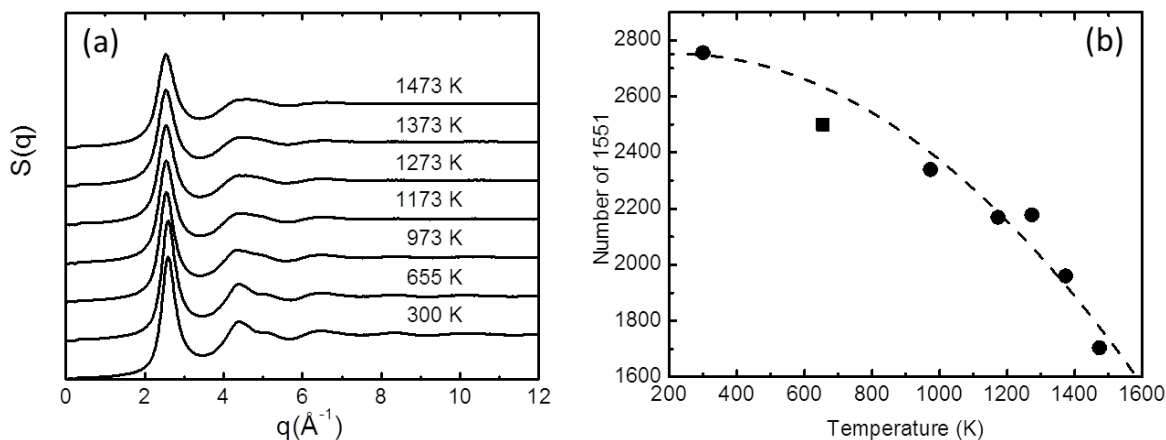
Figure 3 – (a) Experimental $S(q)$ data for liquid $Zr_{59}Ti_3Cu_{20}Ni_8Al_{10}$ as a function of temperature. (b) Number of 1551 HA indices (indicating ISRO) obtained from RMC fits to the $S(q)$ data as a function of temperature.
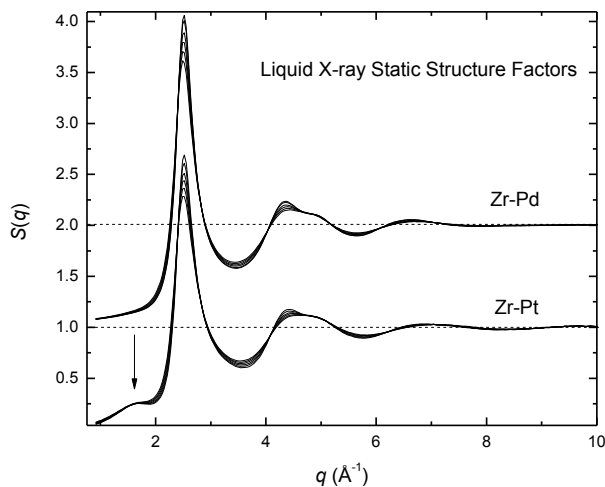
Figure 4 – Liquid X-ray static structure factor for Zr-Pt and Zr-Pd eutectic liquids. For each alloy, a series of $S(q)$'s are plotted corresponding to the temperature range over which the data were collected.

36

III. Thermophysical Property Measurements using ESL

Employing non-contact techniques, WU-BESL can be used to measure thermophysical properties such as density, thermal expansion, specific heat, viscosity and surface tension. A brief discussion of the techniques used for measurements of the density, thermal expansion coefficient and specific heat in WU-BESL is provided here.

Following techniques developed by others [33, 34], the density is measured from video data of the shadow of a levitated sample. A schematic layout of the WU-BESL density measuring system is shown in Fig. 5. Video data are taken at 25 frames per second (fps) with an exposure time of 0.8 ms using a 1.6 megapixel CMOS monochrome camera (pixeLINK®) and a K2/SC long distance video microscope lens, with a close focus objective that is capable of magnifications of 2.13 - 0.71 and a working distance of 222 - 418 mm. A 450 nm band pass having a 40 nm full-width-at-half-max is placed between the camera and the lens system to exclude interference from thermal radiation [34]. The samples are backlit through a transparent port that is opposite to the camera and lens with a 455 nm collimated microscope LED, having a total beam power of approximately 240 mW and a beam diameter of 37 mm. The pixel dimensions are calibrated between studies of samples of each composition using 3/32" diameter grade 3 ($\pm$ 3 x 10^{-5}" diameter) tungsten carbide standards (Industrial Tectonics Inc).
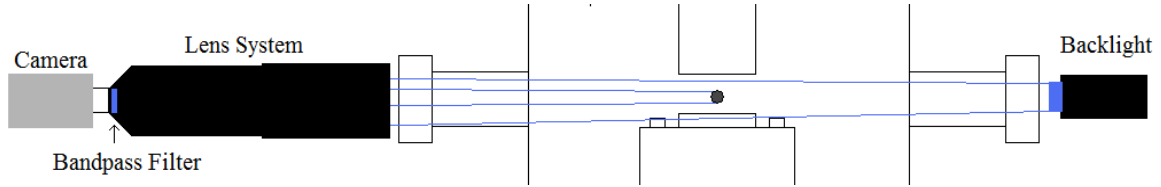
Figure 5 – Schematic diagram for density and volume expansion measurements in WU-BESL.

The video are analyzed to identify the edges of the 2D sample silhouette and then integrated about an axis of symmetry to calculate sample volume, following a method described by Bradshaw et. al. [35]. The coefficient of thermal expansion $\left(\beta = (\partial \ln V / \partial T)_P\right)$ is determined from linear fits to regions of the volume-temperature data. The error in the density is dominated by the uncertainty in the volume and mass calibrations ($\pm$ ~0.4%). These uncertainties cancel in the thermal expansion calculations. There, the dominant contribution to the error are the uncertainty in the temperature calibration (~ $\pm$1%) and the uncertainty in the linear fit to the data (~ $\pm$ 1%), giving a total uncertainty in β of ~ $\pm$ 2%.

For illustration, the measured density of the best glass-forming Cu-Zr liquid ($Cu_{64}Zr_{36}$) during free cooling is shown in Fig. 6.a. The density increases approximately linearly with decreasing temperature (see inset in Fig. 6.a) and can be described by

$$\rho(T) = \left[7.316 \pm .023 \text{ gcm}^{-3}\right]\left[1. + \left(\left[8.57 \pm 0.15\right]\cdot 10^{-5}\text{K}^{-1}\right)\left(994^{\circ}\text{C} - T\right)\right]. \quad (1)$$

Since the sample is levitated in vacuum, when laser power is removed, the sample will cool by radiation loss described by the Stefan-Boltzmann equation, giving

$$mC_P dT/dt = -A\varepsilon\sigma\left(T^4 - T_R^4\right) \quad , \quad (2)$$

where T_R is the effective room temperature of the chamber, A is the sample surface area, ε is the hemispherical emissivity, σ is the Stefan-Boltzmann constant, m is the sample mass, and C_P is the sample specific heat capacity. By determining the temperature derivative from the measured temperature as a function of time during cooling, the ratio C_P/ε is readily obtained. As an example, the C_P/ε values measured as a function of temperature for $Cu_{64}Zr_{36}$ are shown in Fig. 6.b. As observed in other alloy liquids, C_P/ε increases approximately linearly with decreasing temperature, with the rate of increase becoming slower at lower temperatures. Were the emissivity approximately constant across this temperature range, this would suggest a rise in the specific heat, which would be consistent with the ordering of the liquid.
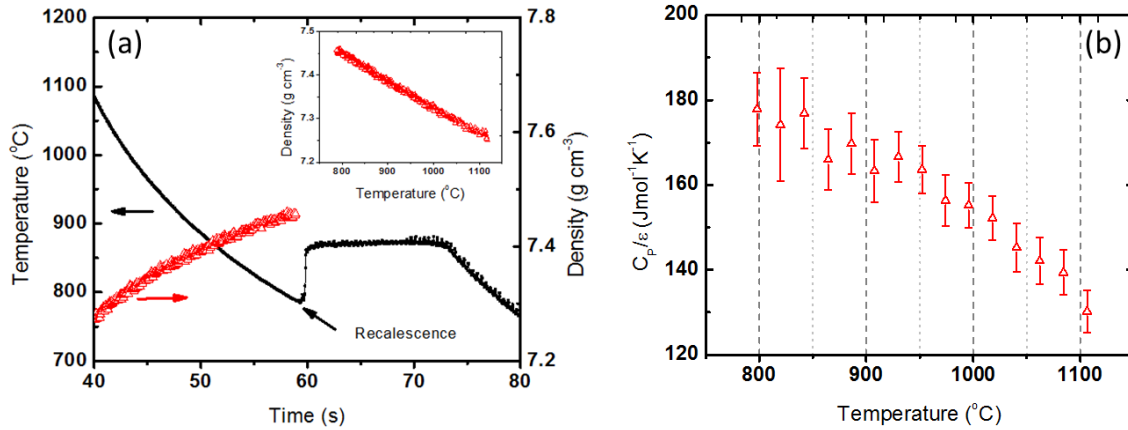
Figure 6 – (a) Temperature as a function of time during free cooling of the sample and the corresponding change in density. The density as a function of temperature is shown in the inset to the figure. (b) Measured C_P/ε as a function of temperature with the estimated error.

IV. Summary and Future Directions

New methods for obtaining structural information have been applied to supercooled metallic glass-forming liquids. These studies have demonstrated that these liquids typically develop significant short-range order, often with an icosahedral character. Some liquids also develop medium-range ordering, extending beyond nearest-neighboring atoms; our studies indicate that this may occur in more metallic liquids than is generally thought. Structural ordering has an impact on phase transitions occurring in the liquid and likely on liquid properties. We have developed capabilities that allow the density, volume expansivity, specific heat, viscosity and surface tension to be measured simultaneously with the structural studies to investigate this.

Since neutrons scatter differently from X-rays, they provide additional information about chemical ordering in a sample. Further, since the neutron scattering cross section differs among

different isotopes, it is possible to obtain additional information from elastic neutron scattering studies on samples made with isotopic substitution. These data can be used to constrain RMC fits to the X-ray scattering data, allowing structures with realistic topological/chemical order to be inferred. Neutron scattering studies can also provide information about dynamics. Due to their lack of periodicity, only long wavelength phonons are present in liquids; the strong temperature dependence of the liquid structure makes it difficult to predict the vibrational properties. Inelastic neutron scattering experiments allow these and related issues in liquids, such as atomic diffusion and the existence of dynamical transitions, like mode-coupling and the glass transition, to be quantitatively investigated. We are currently constructing an ESL for neutron scattering studies (Neutron ESL, NESL). NESL has been designed take full advantage of the high neutron flux and the exceptionally high solid angle detector coverage at several of the beamlines at the Spallation Neutron Source (SNS) at Oak Ridge National Laboratory, including VULCAN, ARCS, CNCS, BASIS and NOMAD.

Using the quiescent microgravity environment on the ISS, experiments are planned to investigate the role of stirring on the amount of supercooling possible in metallic liquids that crystallize to phases of different composition. This will allow the effects of diffusion on the nucleation rate to be studied. Modulated specific heat and other thermophysical property measurements in metallic glass-forming liquids will enable studies of possible liquid/liquid phase transitions and their relation to structure, determined from the ground-based WU-BESL and NESL studies. The results of these studies will improve our knowledge of phase transitions that occur in liquids and help develop methods that can lead to improved microstructural control.

Acknowledgements

References

1.   D. B. Fahrenheit, *Phil. Trans. Roy. Soc.*, **39**(1724) 78-89.
2.   D. Turnbull, *J. Chem. Phys.*, **20**(1952) 411-424.
3.   K. F. Kelton and A.L. Greer, *Nucleation in Condensed Matter - Applications in Materials and Biology*, Pergamon Materials Series (Amsterdam: Elsevier, 2010).
4.   F. C. Frank,*Proc. Roy. Soc. LondonA*, **215** (1952) 43-46.
5.   J. C. Holzer and K.F. Kelton, *Acta Metall. et Mater.*, **39** (1991) 1833-1843.
6.   D. Holland-Moritz, *International Journal ofNon-Equilibrium Processing*, **11** (1998) 169-199.
7.   T. Schenk, D. Holland-Moritz, V. Simonet, R. Bellissent and D.M. Herlach, *Phys. Rev. Lett.*, **89**(2002) 075507/1-4.
8.   K. F. Kelton, G.W. Lee, A.K. Gangopadhyay, R.W. Hyers, T.J. Rathz, J.R. Rogers, M.B. Robinson and D.S. Robinson, *Phys. Rev. Lett.*,**90**(2003) 195504/1-4.
9.   Y. T. Shen, T.H. Kim, A.K. Gangopadhyay and K.F. Kelton, *Phys. Rev. Lett.*, **102** (2009) 057801 /1-4.

10.   K. C. Russell, *Acta Metall.*, **16** (1968) 761-769.
11.   K. F. Kelton, *Acta Mater.*, **48** (2000) 1967-1980.
12.   N. A. Mauro and K.F. Kelton, *Rev. Sci. Instrum.*, **82** (2011) 035114/1-6.
13.   R. L. McGreevy, R.L., *Nuc. Instrum. Methods in Phys. Res. A*, **354** (1995) 1-16.
14.   R. L. McGreevy and J.D. Wicks, *J. Non-Cryst. Solids*, **192-193** (1995) 23-27.
15.   J. D. Honeycutt and H.C. Andersen, *J. Phys. Chem.*, **91** (1987) 4950-4963.
16.   P. J. Steinhardt, D.R. Nelson and M. Ronchetti,*Phys. Rev. B*, **28** (1983) 784-805.
17.   P. J. Steinhardt, D.R. Nelson and M. Ronchetti, *Phys. Rev. Lett.*, **47**(1981) 1297-1300.
18.   J. L. Finney, *Proc. Roy. Soc. London A*, **319**(1970) 479-493.
19.   S. G. Hao, M.J. Kramer, C.Z. Wang, K.M. Ho, S. Nandi, A. Kreyssig, A.I. Goldman, V. Wessels, K.K. Sahu, K.F. Kelton, R.W. Hyers, S.M. Canepari and J.R. Rogers, *Phys. Rev. B*, **79** (2009) 104206/1-7.
20.   G. W. Lee, A.K. Gangopadhyay, K.F. Kelton, R.W. Hyers, T.J. Rathz, J.R. Rogers and D.S. Robinson, *Phys. Rev. Lett.*, **93**(2004) 037802/1-4.
21.   T. H. Kim, G.W. Lee, A.K. Gangopadhyay, R.W. Hyers, J.R. Rogers, A.I. Goldman and K.F. Kelton, *J. Phys. Conden. Matter*, **19**(2007) 452112/1-10.
22.   T.H. Kim and K.F. Kelton, *J. Chem. Phys.*, **126** (2007) 054513/1-7.
23.   N. A. Mauro, J.C. Bendert, A.J. Vogt, J.M. Gewin and K.F. Kelton, *J. Chem. Phys.*, **135**(2011) 044502/1-6.
24.   T. Nakamura, E. Matsubara, M. Sakurai, M. Kasai, A. Inoue and Y. Waseda, *J. Non-Cryst. Solids*, **312-314**(2002) 517-521.
25.   J. M. Park, J.H. Na, D.H. Kim, K.B. Kim, N. Mattern, U. Kuhn and J. Eckert, *Phil Mag.*, **90**(2010) 2619-2633.
26.   W. G. Stratton, J. Hamann, J.H. Perepezko, P.M. Voyles, X. Mao and S.V. Khare, *Appl. Phys. Lett.*, **86**(2005) 141910/1-3.
27.   H. K. Breitzke, Luders, S. Scudino, U. Kuhn and J. Eckert, *Phys. Rev. B*, **70**(2004) 014201/1-12.
28.   A. P. Sokolov, A. Kisliuk, M. Soltwisch and D. Quitmann, *Phys. Rev. Lett.*, **69** (1992) 1540-1543.
29.   B. Xiufang, S. Minhua, X. Xianying and Q. Xubuo, *Mater. Lett.*, **57**(2003) 2001-2006.
30.   J. Saida, M. Matsushita and A. Inoue, *J. Appl. Phys.*, **90** (2001) 4717-4724.
31.   N.A. Mauro, V. Wessels, J.C. Bendert, S. Klein, A.K. Gangopadhyay, M.J. Kramer, S.G. Hao, G.E. Rustan, A. Kreyssig, A.I. Goldman and K.F. Kelton, *Phys. Rev. B*, **83**(2011) 184109/1-8.
32.   N.A. Mauro, W. Fu, J.C. Bendert, Y. Chen, E. Ma and K.F. Kelton, "Local atomic structure in equilibrium and supercooled liquid $Zr_{75.5}Pd_{24.5}$," *Phys. Rev. B*, (submitted).
33.   W.-K. Rhim, S.K. Chung, D. Barber, K.F. Man, G. Gutt, A.J. Rulison and R.E. Spjut, *Rev. Sci. Instrum.*, **64**(1993) 2961-2970.
34.   T. Ishikawa, P.F. Paradis and S. Yoda, *Rev. Sci. Instrum.*, **72**(2001) 2490-2495.
35.   R. C. Bradshaw, D.P. Schmidt, J.R. Rogers, K.F. Kelton and R.W. Hyers, *Rev. Sci. Instrum.*, **76**(2005) 125108/1-8.